Separation Science and Technology
Publication details, including instructions for authors and subscription information:
http://www.informaworld.com/smpp/title~content=t713708471

Cation Exchange and Sorption Properties of Aluminum Phosphate

T. Mishra; K. M. Parida; S. B. Rao

To cite this Article Mishra, T. , Parida, K. M. and Rao, S. B.(1998) 'Cation Exchange and Sorption Properties of Aluminum Phosphate', Separation Science and Technology, 33: 7, 1057 — 1073
To link to this Article: DOI: 10.1080/01496399808545008
URL: http://dx.doi.org/10.1080/01496399808545008

SEPARATION SCIENCE AND TECHNOLOGY, 33(7), pp. 1057–1073, 1998

Cation Exchange and Sorption Properties of Aluminum Phosphate

T. MISHRA, K. M. PARIDA,* and S. B. RAO
REGIONAL RESEARCH LABORATORY
COUNCIL OF SCIENTIFIC & INDUSTRIAL RESEARCH
BHUBANESWAR-751 013, ORISSA, INDIA

ABSTRACT

The ion-exchange properties of amorphous aluminum phosphate have been studied in aqueous electrolyte solutions of KCl over a temperature range of 300–320 K. The data were explained by the law of mass action. Sorption of Cu^{2+}, Ni^{2+}, and Co^{2+} on $AlPO_4$ was also studied as a function of temperature and concentration, and the data were fitted to Langmuir adsorption equations. In all cases the adsorption was found to increase with increases in temperature and concentration in the selectivity order $Cu^{2+} > Co^{2+} > Ni^{2+}$. Further, the values of Langmuir constants were used to calculate the thermodynamic parameters $\Delta S°$, $\Delta H°$, and $\Delta G°$.

Key Words. Ion exchange; Sorption; Aluminum phosphate

INTRODUCTION

The ion-exchange properties of metal phosphates such as zirconium (1, 2), calcium (3), and uranyl phosphates (4) have been studied in great detail due to their high ion-exchange capacity, thermal stability, and resistance to radiation. These materials have been regarded as the best type of exchanger for the separation of radioisotopes and the removal of corrosion products from reactor cooling water (5). However, very little attention has been paid to the sorption

* To whom correspondence should be addressed.

properties of other metal phosphates such as those of iron, aluminum, and titanium.

Aluminum phosphate ($AlPO_4$) has been considered one of the most promising support materials for different catalysts (6, 7). It is of great significance in water purification and also plays an important role in the corrosion of metals and alloys. Although very recently iron (8) and titanium phosphates (9) have been studied as ion exchangers, no report is available on the sorption and ion-exchange properties of aluminum phosphates. The purpose of the present study is to evaluate the ion-exchange and sorption properties of $AlPO_4$ toward Co^{2+}, Ni^{2+}, and Cu^{2+} as a function of temperature and concentration.

EXPERIMENTAL

Sample Preparation

Aluminum phosphate was prepared by a coprecipitation method using 1 : 1 ammonia as a precipitating agent. Aqueous solutions (500 mL) of aluminum chloride (0.2 M) and orthophosphoric acid (0.2 M) were taken in a 1-L beaker and stirred with a magnetic paddle. Then ammonia solution was added dropwise until the pH of the solution became 7.5. The precipitate thus formed was filtered, washed, and dispersed in 2-propanol for 1 hour. It was again filtered and dried at 120°C. The dried products were sieved, and the sieve fractions from −75 to +45 mm were collected. Then the powder was calcined at 600°C as in our previous study (10). The calcined sample (600°C) showed the highest surface area, pore volume, and surface acidity. About 100 mg of the sample was dissolved in 10 mL HCl (1 : 1) and made up to the mark in a 100-mL volumetric flask. The amount of aluminum in the solution was determined by atomic absorption spectroscopy while the phosphate was estimated spectrophotometrically at $\lambda = 430$ nm by forming the phosphovanado molybdate complex.

Textural Properties

Powder XRD patterns of the samples were recorded with a Philips (model 1710) semiautomatic x-ray diffractometer with an autodivergent slit and with a graphite monochromator using CuKα radiation with a scanning speed of $2°\cdot min^{-1}$.

Thermograms of the air-dried sample were carried out in dry air using a Shimadzu DT40 Thermal Analyser in the 50–1000°C temperature range at a heating rate of $10°C\cdot min^{-1}$.

Surface area, pore volume, average pore diameter, and pore size distribution were determined by the nitrogen adsorption–desorption method at liquid nitrogen temperature using a Quantasorb surface area analyzer (Quantachrome,

USA). Prior to the adsorption–desorption measurements the sample was degassed at 200°C and 10^{-5} torr for 12 hours.

FT-IR spectra were recorded with a Jasco FT-IR spectrometer in the 4000–400 cm^{-1} range in the KBr phase. Prior to the analysis the sample was degassed at 120°C in vacuum (1×10^{-4} torr).

Potentiometric Titration of Aluminum Phosphate

Potentiometric titrations of aluminum phosphate samples in 0.1 $mol \cdot dm^{-3}$ KCl solution at different temperatures (300–320 K) were carried out in a thermostated double-walled glass cell of 100 mL capacity with a cork lid containing the electrode and a microburette.

For each experiment 25 mL of electrolyte (KCl) and 0.1 g of sample were taken in the cell with constant stirring until the pH became constant. After equilibrium the pH of the suspension was measured by an Elico Digital pH-meter (model LI 120), and then standard 0.01 $mol \cdot L^{-1}$ KOH solution was added dropwise with a microburette. The pH of the suspension was recorded when the pH drift was less than 0.01 units/min. Likewise, the addition of KOH and the measurement of pH was continued until the pH reached 9.

Adsorption of Metal Ions on Aluminum Phosphate

The adsorption of transition metal ions (Co^{2+}, Ni^{2+}, and Cu^{2+}) was carried out from 50 mL of the solution in a 100-mL stoppered flask. The initial pH of the solution was measured. Then 0.1 g aluminum phosphate was added and the resulting suspensions were shaken mechanically with the help of a Julabo-shaker for 24 hours. Preliminary experiments revealed that 24 hours is required for the system to reach equilibrium. Then the suspension was filtered and the equilibrium pH of the filtrate was measured. In all the experiments the pH remained within the 4 to 4.8 range. The concentration of metal ions in the filtrate was determined with an atomic absorption spectrometer. The difference in pH between the initial and final solutions was used to calculate the stoichiometry of the ion-exchange reaction. The adsorption experiment was repeated at four different concentrations (8.00, 6.00, 4.00, 2.00) $\times 10^{-4}$ $mol \cdot dm^{-3}$ of Co^{+2}, Ni^{+2}, and Cu^{+2}. The results were reproducible within $\pm 6\%$.

RESULTS AND DISCUSSION

Chemical Analysis and X-ray Diffraction

Chemical analysis showed that the P/Al ratio in the sample is less than 1 (0.951), although during preparation the ratio was kept at 1 in the solution. In this process aluminum hydroxide is first precipitated and subsequently

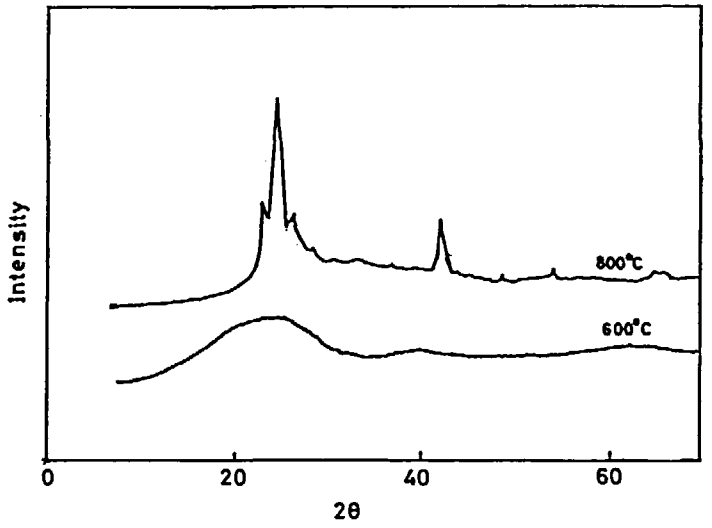

FIG. 1 XRD patterns of $AlPO_4$ calcined at 600 and 800°C.

converted to $AlPO_4$. So, invariably, some part of the aluminum hydroxide remains with the $AlPO_4$ which on calcination becomes Al_2O_3 (10). The x-ray diffraction pattern (Fig. 1) shows that the material is amorphous in nature after calcination at 600°C. Crystallinity increases with increasing temperature, and at 800°C it becomes crystalline.

Surface Area and Porosity

The BET surface area of the sample calcined at 600°C is 203 m^2/g whereas for the sample calcined at 120°C it is only 102 m^2/g. This increase in surface area is accompanied by an increase in porosity (pore volume became 0.267 mL/cm^3). Assuming the pores to be cylindrical, the average pore radius is calculated by using the formula $d = 4V_p/S_p$, where d is the average pore diameter, V_p is the volume of pores, and S_p is the specific internal surface area of the pores. From this calculation, d is found to be 26.3 Å. Pore size distribution calculated using the BJH equation (11) is presented in Fig. 2, which shows the predominant presence of pores in the same range.

Thermogravimetric Analysis

It is evident from the thermogravimatric analysis (TG) curve (Fig. 3) that the major weight loss of 22.5% occurs at around 140–280°C, which is in

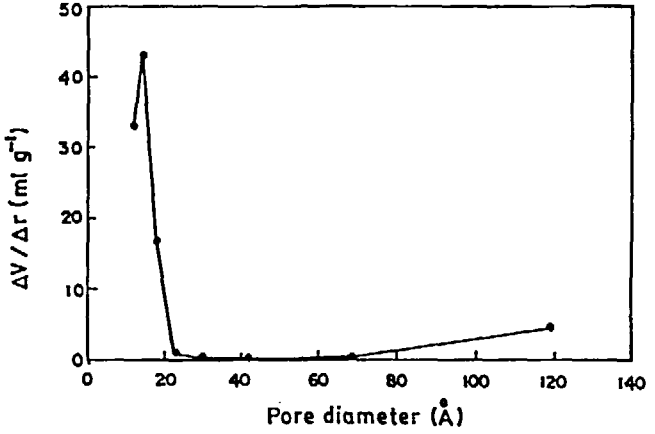

FIG. 2 Pore size distribution of $AlPO_4$ calcined at 600°C as a function of pore diameter.

accordance with the reaction $AlPO_4 \cdot 2H_2O \rightarrow AlPO_4 + 2H_2O$, which accounts for a 25% weight loss. Around 3.5% weight loss occurred between 280 and 700°C, which may be due to the loss of strongly bonded water molecules. However, there is enough overlap between the two temperatures so the loss cannot be quantified exactly. Above 700°C the TG curve flattens, with a gradual weight loss up to 995°C. The last part of the DTA curve associated with an endotherm which may be due to the phase transformation of amorphous to crystalline as observed in earlier work (10). This suggests

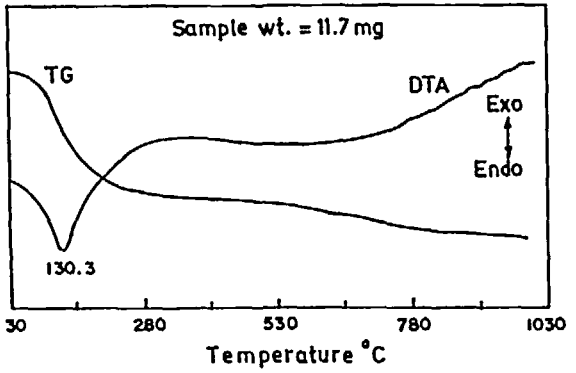

FIG. 3 TG/DTA analysis of $AlPO_4$ dried at room temperature.

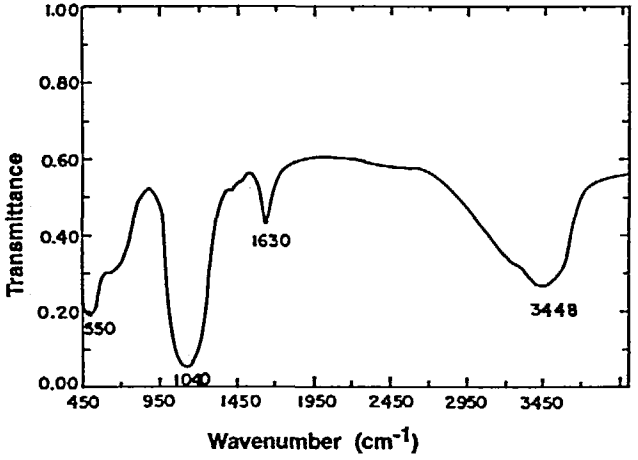

FIG. 4 FT-IR spectra of $AlPO_4$ calcined at 600°C.

that the material at 600°C calcination retains its surface hydroxyl groups which are probably responsible for the ion-exchange properties.

FT-IR Spectra

The FT-IR spectra of an aluminum phosphate sample calcined at 600°C is presented in Fig. 4. The band at 550 cm^{-1} can be assigned to the Al—O stretching or P—O—H bending vibration, whereas the band at 1040 cm^{-1} is due to P—O—H stretching. The broad bands at 1630 and 3448 cm^{-1} correspond to O—H bending and stretching vibrations, respectively (1).

Potentiometric Titration

Potentiometric titration curves of aluminum phosphate calcined at 600°C in 0.1 mol·dm^{-3} KCl at different temperatures (300, 310, and 320 K) are presented in Fig. 5. They suggest that the pH of the suspension increases with the addition of KOH, which is in contrast to other systems (12) where the pH remains constant with ion uptake. Further, there is no break or end point in the curves, showing $AlPO_4$ to be a weak monobasic acid. This type of behavior was also observed with a weakly acidic ion exchanger like zirconium phosphate (13). Interestingly, the curves show that the pH of the solution shifts toward lower values with an increase in temperature. This indicates that H^+ liberation is facilitated by an increase in temperature, which can be expressed in the following reaction:

$$n\mathrm{RH} + \mathrm{M}_{aq}^{x+} \leftrightharpoons \mathrm{R}_n\mathrm{M}^{x-n} + n\mathrm{H}_{aq}^{+} \quad (1)$$

where RH is the exchanger and M^{x+} is the metal ion. This shows that with an increase in temperature, more and more H^+ ions are displaced by the K^+ ions. Hence, sorption of the K^+ ion increases with temperature.

Figure 6 shows that the titration curve of $AlPO_4$ in KCl in the presence of Ni^{2+} shifts the pH to a lower value in comparison to the blank titration, which was also observed in the case of α-aluminum hydroxides (14). Thus, the mechanism of metal-ion uptake in this case is similar to that of adsorption on oxides or hydroxides which can be described by Eq. (1). The amount of replaceable protons responsible for the ion-exchange reaction can be estimated from the difference between the blank run and each titration curve in the presence of the exchanger. Thus, the ratio of the excess amount of base

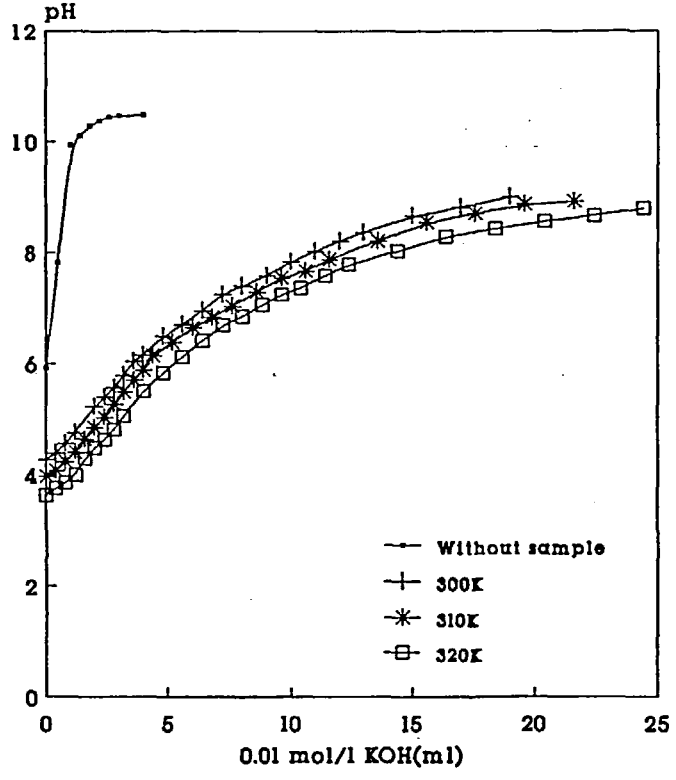

FIG. 5 Potentiometric titration of $AlPO_4$ aqueous solution of 0.1 mol·L^{-1} KCl at different temperatures.

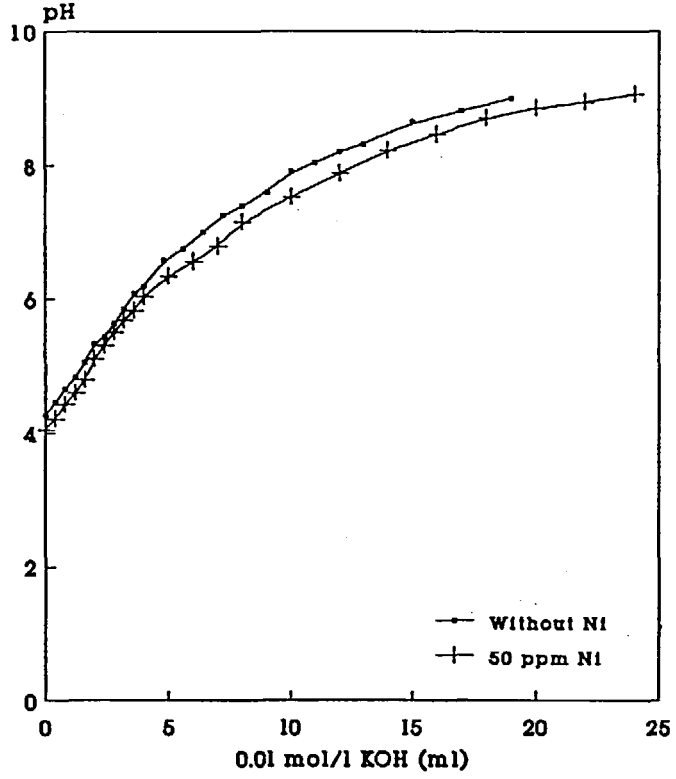

FIG. 6 Potentiometric titration of $AlPO_4$ in aqueous solution of 0.1 mol·L^{-1} KCl in the presence of 50 ppm Ni^{2+} solution at 300 K.

consumed in the presence of $AlPO_4$ gives the extent of sorption of metal cations. Therefore, Eq. (1) can be rewritten as follows by applying the law of mass action:

$$K = \frac{[(R)_n M^{x-n}][H^+]^n}{[RH]^n[M^{x+}]} \tag{2}$$

where K is the equilibrium constant and the symbols in brackets represent the respective concentrations. In the region of low adsorption, $[RH]^n$ and $[M^{x+}]$ can be treated as constants and $[(R)_n M^{x-n}]$ is equal to Cb/n, where Cb is the volume of 0.01 mol·L^{-1} of KOH added. Thus, Eq. (2) can be simplified to

$$K = [Cb/n][H^+]^n \tag{3}$$

or

$$\log Cb = \log Kn + n\text{pH} \quad (4)$$

By using Eq. (4), log *Cb* vs pH can be plotted to determine log *K* and *n*. Plots of log *Cb* as a function of pH for the potentiometric titration of K^+ ions are presented in Fig. 7. From these plots log *K* and *n* were calculated and the results are presented in Table 1. Interestingly, the curves in Fig. 7 shows two distinct lines, indicating the complex mechanism of K^+ ion sorption by $AlPO_4$. This complication in the plot clearly indicates the inadequacy of Eq. (4) with the simplifying assumption as well as the presence of different types of exchange sites on $AlPO_4$. This results also shows that Eq. (4) is only applicable within pH 3 to 5, indicating the limitation of the simplification. Therefore, the equation is more appropriate at a low adsorption density. Interestingly, the break point is nearly the same for all three plots: log *Cb* =

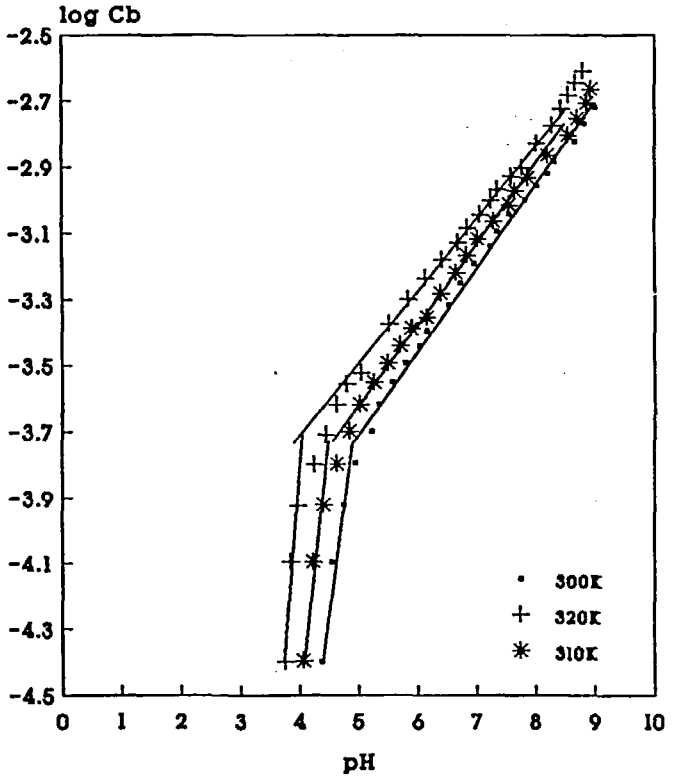

FIG. 7 Plots of log *Cb* vs pH for $AlPO_4$ in aqueous solution of 0.1 mol·L^{-1} KCl at different temperatures.

TABLE 1
Values of Log K and n Calculated from Eq. (4) for K^+ Exchange on $AlPO_4$

Sample	Temperature (K)	Log K	n
$AlPO_4$	300	−10.83	1.00
$AlPO_4$	310	−10.99	1.1
$AlPO_4$	320	−11.07	1.30

−3.70 to −3.75. This probably shows that the number of high energy sites responsible for the uptake of K^+ ions is independent of temperature (300–320 K). The value of n determined (Table 1) from the line within the low pH region is nearly equal to 1, which suggests the ion-exchange stoichiometry for alkali-metal ions is

$$RH + M^+ = RM + H^+ \quad (5)$$

Adsorption of Heavy-Metal Ions

Preliminary experiments showed that the adsorption capacity of the sample calcined at 600°C toward Cu^{2+}, Co^{2+}, and Ni^{2+} is higher than the sample calcined at 120°C (Fig. 8). Adsorption of bivalent transition metals at different temperatures and concentrations on aluminum phosphate calcined at 600°C shows that the uptake increases with increases in concentration and temperature for all the metal ions. The representative plot of Cu^{2+} adsorption on $AlPO_4$ is presented in Fig. 9. The order of selectivity of $AlPO_4$ toward the metal ions is $Cu^{2+} > Co^{2+} > Ni^{2+}$. This order was also reported for α-zirconium phosphate (15) and hydrous MnO_2 (16). But in the case of antimonic acid (17), a different order was followed, which was explained on the basis of the stability of hexaquo ions. It was stated earlier (18) that in the case of zirconium phosphates, this order can neither be related to the stability of hexaquo ions nor to the stereochemistry adopted by M^{2+} ions in the solid. Of course, the stereochemistry of M^{2+} on the surface of the $AlPO_4$ cannot be compared with that of $ZrPO_4 \cdot 4H_2O$ due to their structural differences. However, comparing the extent of sorption of metal ions with the ionic potential and hydrolysis constant (K_h) of the metal cations in solution, the ion exchanger prefers the cation with a low ionic potential and a low pK_h value. As Cu^{2+} has the lowest pK_h (= 8.0), the adsorption is larger in comparison to Co^{2+} (pK_h = 8.9) and Ni^{2+} (pK_h = 9.9) (19).

The ratios of H^+ released to M^{x+} adsorbed for all the metal ions are slightly more than 2 (Table 2). It can be concluded that, on average, 2 moles of H^+ ions are released per mole of metal ion adsorbed. This type of observation was

also reported for the adsorption of various bivalent cations on oxide/hydroxide surfaces (20–22). Therefore, the exchange reaction can be expressed as

$$2RH + M^{2+} = R_2M + 2H^+ \quad (6)$$

where RH is the exchanger and R_2M is the exchanged form.

The adsorption data were fitted to linearly transformed Langmuir adsorbed isotherms:

$$Ceq/X = (1/bXm) + Ceq/Xm \quad (7)$$

where *Ceq* is the equilibrium concentration of adsorbate in solution (mol/L), *X* is the amount of adsorbate per unit mass of adsorbent (mol/g), *Xm* is the amount adsorbed to form a monolayer (mol/g), and *b* is the binding constant.

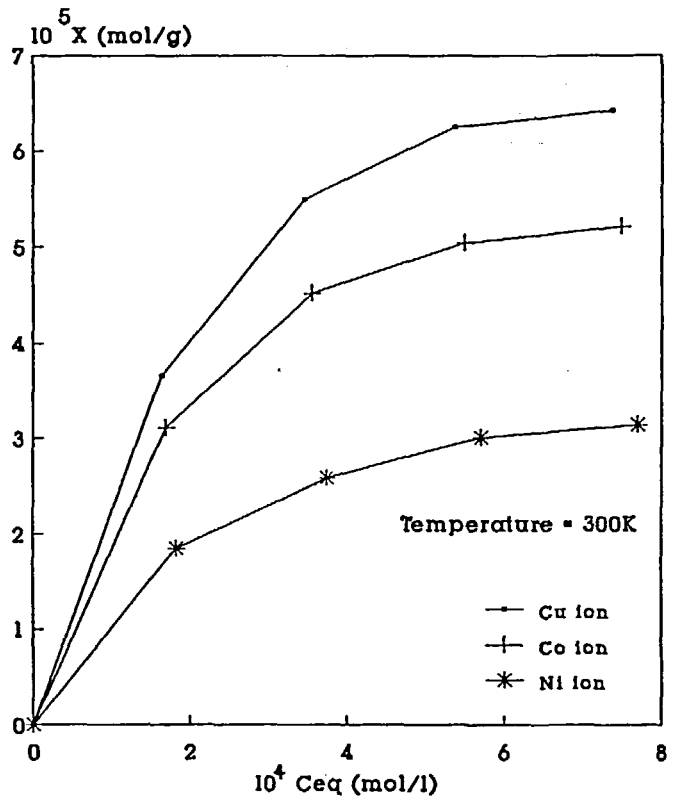

FIG. 8 Adsorption isotherms of Cu^{2+}, Co^{2+}, and Ni^{2+} on $AlPO_4$ sample calcined at 120°C.

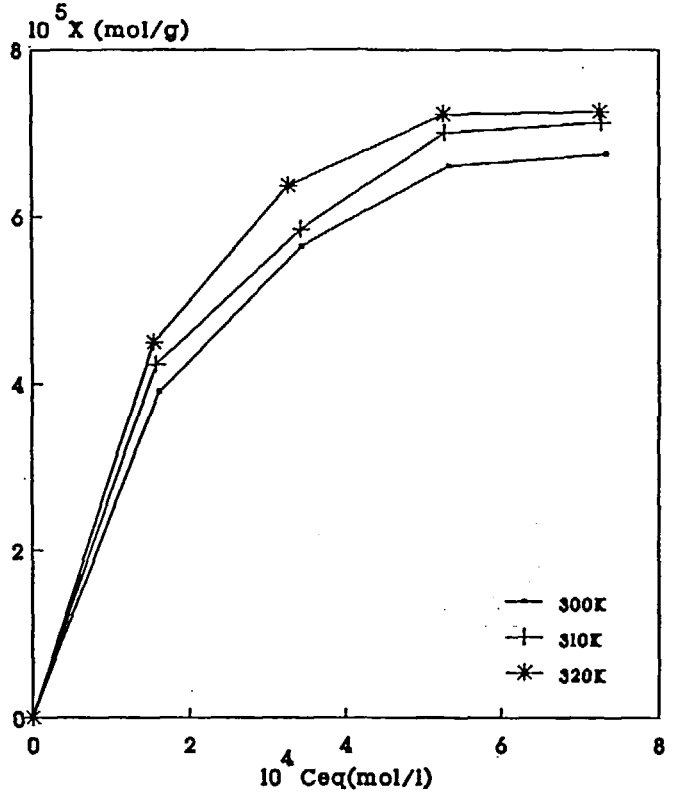

FIG. 9 Adsorption isotherms of Cu^{2+} at different temperatures on $AlPO_4$ calcined at 600°C.

Plots of *Ceq/X* vs *Ceq* give straight lines (Fig. 10) at all temperatures, with a correlation coefficient > 0.99 (Table 5), which favors the applicability of the Langmuir equation within pH 4 to 5. The values of *Xm* and *b* as determined from the plots are tabulated in Tables 3 and 4. Both values increase with increasing temperature, indicating the endothermic nature of the adsorption. The apparent equilibrium constants (K_a) corresponding to the adsorption process were calculated (23) as the product of the Langmuir parameters *b* and *Xm* and can be used as relative indicators of the affinity of the adsorbents toward the metal ions. The data (Table 5) show that the affinity of $AlPO_4$ toward the metal ions increases with an increase in temperature. From the plots of ln *b* vs T^{-1} (Fig. 11), the standard enthalpy and entropy changes were calculated by using Eq. (8):

$$\ln b = \Delta S°/R - \Delta H°/RT \quad (8)$$

By using the $\Delta S°$ and $\Delta H°$ values in Eq. (9), the Gibbs free energy change ($\Delta G°$) can be calculated.

$$\Delta G° = \Delta H° - T\Delta S° \quad (9)$$

All the values of $\Delta S°$, $\Delta H°$, and $\Delta G°$ are tabulated in Tables 6 and 7. They show that $\Delta H°$ and $\Delta S°$ are positive and $\Delta G°$ is negative for all the experiments. The positive values of $\Delta H°$ and $\Delta S°$ indicate the endothermic nature and increased disorderliness in the system, respectively. Also, a large amount of heat is required to remove the hydrated bivalent metal ions from solution. Therefore, the adosrption process becomes endothermic. The positive value of $\Delta S°$ indicates the partial dehydration of the metal ions before adsorption, thus increasing the spontaneity. Again, both the $\Delta H°$ and $\Delta S°$ values follow the same order ($Cu^{2+} > Co^{2+} > Ni^{2+}$) as the selectivity shown by the exchanger. The same order was found for $FePO_4$ (8), but in the case of antimonic acid a reverse order was followed ($Co^{2+} > Ni^{2+} > Cu^{2+}$) (24). From these results it can be concluded that changes in the hydration of a metal cation play the dominant role in determining the selectivity of the exchanger. The highest disorder of the system was for Cu^{2+} (Table 6), which shows that Cu^{2+}

TABLE 2
Stoichiometry of Metal Ion Exchange on $AlPO_4$ at Different Concentrations at 300 K

Initial metal ion concentration (10^{-4} mol·L^{-1})	Equilibrium concentration *Ceq* (10^{-4} mol·L^{-1})	Metal ion adsorbed (10^{-5} mol·L^{-1})	H^+ released (10^{-5} mol·L^{-1})	H^+/M^{2+}
		Cu^{2+} adsorption		
2	1.61	3.9	8.21	2.1
4	3.435	5.65	11.92	2.11
6	5.339	6.61	13.5	2.05
8	7.324	6.76	14.05	2.07
		Co^{2+} adsorption		
2	1.67	3.3	6.72	2.03
4	3.518	4.82	10.06	2.08
6	5.46	5.40	10.99	2.03
8	7.455	5.457	11.01	2.01
		Ni^{2+} adsorption		
2	1.79	2.1	4.52	2.15
4	3.726	2.74	5.74	2.09
6	5.686	3.14	6.46	2.05
8	7.678	3.22	6.89	2.13

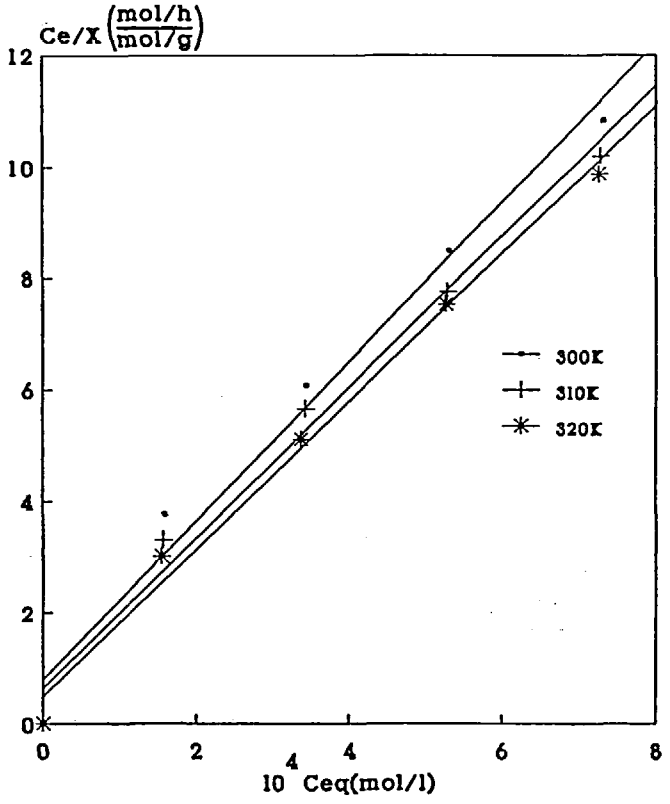

FIG. 10 Langmuir plots for the adsorption of Ni^{2+} on $AlPO_4$ at different temperatures.

TABLE 3
Langmuir Parameter *Xm* ($mol \cdot g^{-1}$)

Sample	Temperature (K)	10^5 *Xm*		
		Cu^{2+}	Co^{2+}	Ni^{2+}
$AlPO_4$	300	6.82	5.20	3.2
$AlPO_4$	310	7.11	5.59	3.47
$AlPO_4$	320	7.21	5.98	3.61

TABLE 4
Langmuir Constant b for the Metal Ion Exchange on $AlPO_4$

Sample	Temperature (K)	Cu^{2+}	Co^{2+}	Ni^{2+}
$AlPO_4$	300	8724	8394	8198
$AlPO_4$	310	9390	8742	8500
$AlPO_4$	320	10284	9339	8936

TABLE 5
Apparent Equilibrium Constant (K_a) and Correlation Coefficient Calculated from Langmuir Equation

		K_a			Correlation coefficient		
Sample	Temperature (K)	Cu^{2+}	Co^{2+}	Ni^{2+}	Cu^{2+}	Co^{2+}	Ni^{2+}
$AlPO_4$	300	0.595	0.436	0.262	0.9996	0.9953	0.9995
$AlPO_4$	310	0.668	0.489	0.295	0.9995	0.9971	0.9994
$AlPO_4$	320	0.741	0.558	0.323	0.9997	0.9991	0.9997

TABLE 6
Entropy and Enthalpy Changes of Metal Ions Exchanged on $AlPO_4$

Sample	Metal ions	$\Delta S°$ ($J \cdot K^{-1} \cdot mol^{-1}$)	$\Delta H°$ ($K \cdot J \cdot mol^{-1}$)
$AlPO_4$	Cu^{2+}	97.69	7.89
$AlPO_4$	Co^{2+}	88.96	3.74
$AlPO_4$	Ni^{2+}	85.63	2.91

TABLE 7
Gibbs Free Energy Change of Metal Ions Exchanged on $AlPO_4$ as a Function of Temperature

		$\Delta G°$ ($K \cdot J \cdot mol^{-1}$)		
Sample	Temperature (K)	Cu	Co	Ni
$AlPO_4$	300	−21.42	−22.95	−22.77
$AlPO_4$	310	−22.34	−23.84	−23.63
$AlPO_4$	320	−22.37	−24.73	−24.48

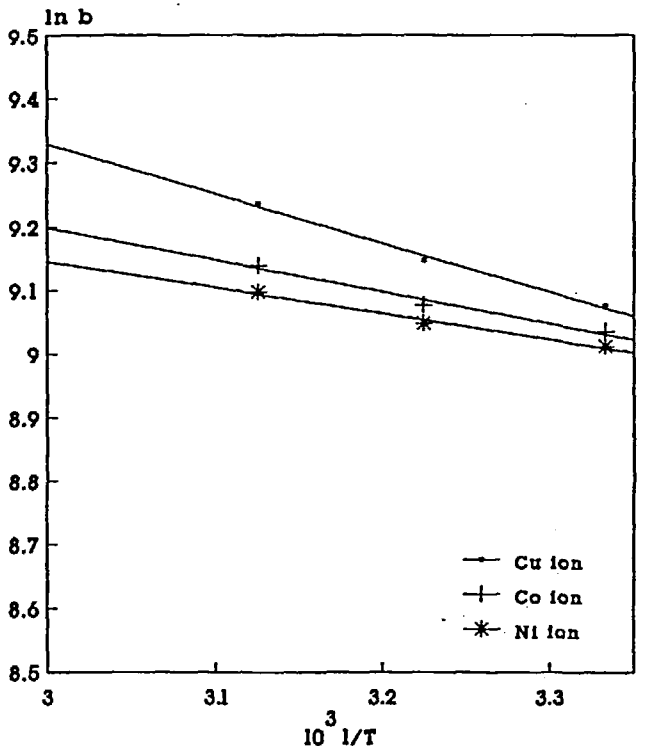

FIG. 11 Plots of ln b vs T^{-1} for different metal ions.

ions lose most of their water of hydration. This is also supported by the highest value of $\Delta H°$ in the series, which indicates that higher energy is needed to dehydrate the Cu^{2+} ions than the Ni^{2+} ions. The value of $\Delta G°$ becomes more negative with increasing temperature. This shows that the adsorption is favored by an increase in temperature.

CONCLUSIONS

From this study it is clear that $AlPO_4$ behaves as a weakly acidic ion exchanger and has an adsorption capacity toward the bivalent transition metal ions Cu^{2+}, Co^{2+}, and Ni^{2+} in the following selectivity order: $Cu^{2+} > Co^{2+} > Ni^{2+}$. As in the case of a weakly acidic exchanger, the change in hydration of metal ions plays the dominant role in determining the selectivity. In all cases the extent of adsorption increases with increases in temperature and

concentration. Although its cation exchange capacity is low, amorphous aluminum phosphate can be used as an cation exchanger like the metal(IV) phosphates.

ACKNOWLEDGMENTS

The authors are thankful to Prof. H. S. Ray, Director, Regional Research Laboratory, Bhubaneswar - 751 013 for his permission to publish this paper. T.M. is thankful to CSIR for providing a fellowship.

REFERENCES

1. S. Allulli, C. Ferragina, A. Ginestra, M. A. Massucci, and N. Tomassini, *J. Chem. Sec., Dalton Trans.*, p. 1979 (1977).
2. S. Ahrland, N. Bjorh, R. H. Blessing, and R. G. Herman, *J. Inorg. Nucl. Chem.*, *36*, 2377 (1974).
3. K. A. Kraus and H. O. Phillips, *J. Am. Chem. Soc.*, *78*, 644 (1956).
4. V. Pekavek and M. Benesova, *J. Inorg. Nucl. Chem.*, *26*, 1743 (1964).
5. N. Souka, R. Shabana, and K. Farah, *J. Radioanal. Chem.*, *33*, 315 (1976).
6. G. Alberti, P. Cardini-Galli, U. Castantiono, and E. Torracea, *J. Inorg. Nucl. Chem.*, *29*, 571 (1967).
7. S. Mustafa, A. N. Khan, and N. Rehana, *J. Chem. Soc., Faraday Trans.*, *89*, 3843 (1993).
8. J. M. Campelo, J. M. Marinas, S. Mendioroz, and J. A. Pajares, *J. Catal.*, *101*, 484 (1986).
9. B. Rebenstorf, T. Linhlad, and S. L. T. Andersson, *Ibid.*, *128*, 293 (1991).
10. K. M. Parida and T. Mishra, *J. Colloid Interface Sci.*, *179*, 233 (1996).
11. E. P. Barrett, L. G. Joyner, and P. P. Halenda, *J. Am. Chem. Soc.*, *73*, 373 (1951).
12. L. Kullberg and A. Clearfield, *J. Phys. Chem.*, *85*, 1585 (1981).
13. A. Clearfield, A. Oskarsson, and C. Oskarsson, *Ion Exch. Membr.*, *1*, 9 (1972).
14. S. Mustafa, M. Safdar, and S. Y. Hussain, *J. Surf. Sci. Technol.*, *5*, 267 (1989).
15. A. Clearfield and J. M. Kalnims, *J. Inorg. Nucl. Chem.*, *38*, 849 (1976).
16. J. M. Gray and M. A. Malati, *J. Chem. Tech. Biotechnol.*, *29*, 135 (1979).
17. M. Abe, K. Yoshigasaki, and T. Sugiura, *J. Inorg. Nucl. Chem.*, *42*, 1753 (1980).
18. S. Allulli, C. Ferragina, A. La Ginestra, M. A. Massucci, and A. G. Tomlinson, *J. Chem. Soc., Dalton Trans.*, p. 2115 (1976).
19. D. D. Perrin and B. Dempsey, *Buffer for pH and Metal Ion Control*, Chapman & Hall, London, 1974.
20. C. P. Huang and W. Sfumm, *J. Colloid Interface Sci.*, *213*, 409 (1973).
21. S. Mustafa and S. K. Khan, *J. Surf. Sci. Technol.*, *7*, 273 (1991).
22. H. M. Jang and D. W. Fuenstenau, *Colloids Surf.*, *21*, 235 (1986).
23. J. D. Lopez-Gonzalez, C. Valenzuela-Aluhorro, T. Jimenez-Lopez, and A. Ramierez-Saenz, *An. Quim.*, *74*, 225 (1978).
24. M. Abe and K. Sudoh, *J. Inorg. Nucl. Chem.*, *42*, 105 (1980).

Received by editor May 25, 1997
Revision received September 1997